J Infrared Milli Terahz Waves manuscript No.
(will be inserted by the editor)

3D printed prisms with tunable dispersion for the THz frequency range

Stefan F. Busch · Enrique Castro-Camus · Felipe Beltran-Mejia · Jan C. Balzer · Martin Koch

Received: date / Accepted: date

Abstract Here, we present a 3D printed prism for THz waves made out of an artificial dielectric material in which the dispersion can be tuned by external compression. The artificial material consists of thin dielectric layers with variable air spacings which has been produced using a fused deposition molding process. The material properties are carefully characterized and the functionality of the prisms is in a good agreement with the underlying theory. These prisms are durable, lightweight, inexpensive and easy to produce.

1 Introduction

Many polymers are reasonably transparent to THz radiation for optical device purposes [1]. Consequently, some devices use these materials in order to effectively manipulate the radiation field. Examples of such devices are lenses [2–4], beam-shapers [5], waveguides [6–10], gratings [11–13] and splitters [14, 15] to name only a few. Additionally, most polymers have a very low or nearly zero dispersion in the THz frequency range. This attribute can be useful for the devices mentioned above. Yet, dispersive materials are important for wavelength demultiplexing, beam shaping, spectroscopy and imaging systems. On previous reports, waveguide dispersion was used to mimic the dispersive behavior of a prism [16]. Others have used a

S.F. Busch and M. Koch
Department of Physics, Philipps University of Marburg
Renthof 5, 35032 Marburg, Germany

E. Castro-Camus
Centro de Investigaciones en Optica A.C., Loma del Bosque 115, Lomas del Campestre, Leon, Guanajuato 37150, Mexico

F. Beltran-Mejia
National Institute of Telecommunications – Inatel
Av. Joao Camargo 510, 37540-000 Santa Rita do Sapucai/MG, Brazil
E-mail: felipebm@inatel.br

Jan C. Balzer
Faculty of Engineering, University of Duisburg-Essen
Bismarckstr. 81, 47057 Duisburg, Germany

hexagonal photonic crystal in order to induce a super-prism effect in the THz regime [17]. Similarly, a quasi-Wollaston prism for polarization splitting was 3D-printed in [18]. Also in [19], a metal parallel-plate waveguide is reported to have a strong frequency-angle dependence. Previously, the form-birefringence of stacked dielectric layers has previously been used for the production of waveplates in the optical [20, 21] and THz regimes [22, 23]. Here, we fabricate a terahertz prism by exploiting the dispersive behavior of such layered media as shown in Fig. 1.

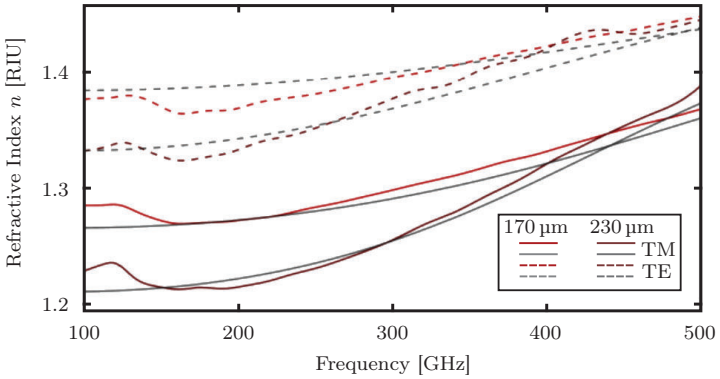

Fig. 1 THz TDS refractive index measurements obtained from two samples with different air spacing: 230 µm (dark red) and 170 µm (light red). Dashed and solid lines represent TE and TM input polarizations respectively. Gray lines illustrates the simulated results for a constant refractive index of $n = 1.56$ obtained by using a plane wave modal solver. [24]

The artificial material consists of a 3D printed array of thin Polystyrene (PS) slabs periodically separated by air as shown on the left side of Fig. 2. Even though both materials show no dispersive behavior, the composite material shows strong dispersion. By modeling the dielectric system according to the coupled mode theory presented by [25], the dispersive behavior can be attributed to the waveguide dispersion of numerous coupled dielectric slab waveguides, as briefly explained in the following section. The measurements and results that support our assumptions are presented in section 3. Finally, we discuss the results and our conclusions along with the future perspectives.

2 Theory

To describe the propagation of an electromagnetic wave along the slabs, we make use of the matrix approach presented by Yeh [25]. Even though the number of layers illuminated in the real experiment is finite, we consider the case of an infinite stack of layers for modeling purposes. According to Yeh, the refractive index profile can be described as,

$$n(x) = n_i : x_i < x < x_{i+1}, \tag{1}$$

where n_i is a constant refractive index of the i-th layer, and x_i represents the position of the periodically spaced interfaces over the x-axis. The whole system can

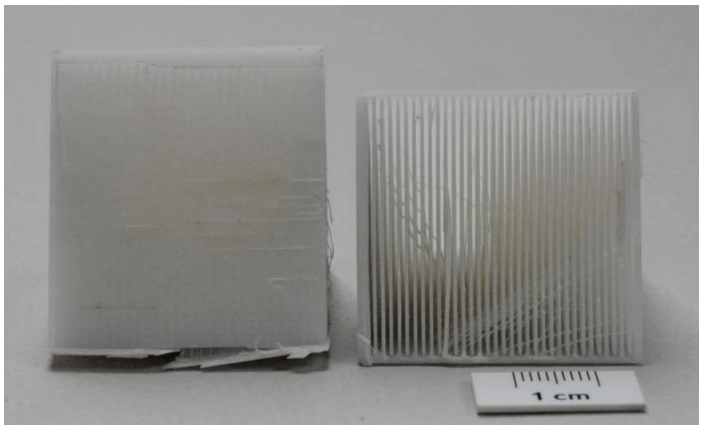

Fig. 2 Picture of two 3D printed prisms using 400 µm layers made of polystyrene and a fixed distance between the PS layers. The smooth input surface can be observed on the left side of the image next to the bottom view of the prism with the cover layer removed.

be described by the transmission matrix M_B. This matrix describes the transition of the electric field between consecutive layers. Owing to the periodic structure of the system, the solution for the electric field has to be periodic as well. The electric field inside each layer can be represented by a right and left propagating part with complex amplitudes A_i and B_i respectively. Then, the electrical field is tied to the electric field of the neighboring layers by M_B,

$$\begin{pmatrix} A_i \\ B_i \end{pmatrix} = M_B \cdot \begin{pmatrix} A_{i-1} \\ B_{i-1} \end{pmatrix}. \tag{2}$$

The matrix M_B is defined by the product,

$$M_B = D_{\mathrm{Air},i} P_{\mathrm{Air},i} D^{-1}_{\mathrm{Air},i} D_{\mathrm{PS},i} P_{\mathrm{PS},i} D^{-1}_{\mathrm{PS},i}, \tag{3}$$

where D and P are the interlayer and intralayer transition matrices given by,

$$D_i^{\mathrm{TE}} = \begin{pmatrix} 1 + ik_{x,i} & 1 - ik_{x,i} \\ 1 - ik_{x,i} & 1 + ik_{x,i} \end{pmatrix}, \tag{4}$$

for TE-polarization, and

$$D_i^{\mathrm{TM}} = \begin{pmatrix} 1 + \frac{n_2^2}{n_1^2} ik_{x,i} & 1 - \frac{n_2^2}{n_1^2} ik_{x,i} \\ 1 - \frac{n_2^2}{n_1^2} ik_{x,i} & 1 + \frac{n_2^2}{n_1^2} ik_{x,i} \end{pmatrix}, \tag{5}$$

for TM-polarization and

$$P_i = \begin{pmatrix} e^{-ik_{x,i}d_i} & 0 \\ 0 & e^{ik_{x,i}d_i} \end{pmatrix}, \tag{6}$$

where $k_{x,i}$ is the cutoff wavenumber of the i-th layer and d is the thickness of the layers.

Due to the periodic structure of the two material system, the solution of the electric field and therefore of the propagation constant can be determined by solving the Bloch-Eigenvalue equation,

$$e^{iK\Lambda}\begin{pmatrix}A_i\\B_i\end{pmatrix} = M_B \cdot \begin{pmatrix}A_i\\B_i\end{pmatrix}, \tag{7}$$

where K is the Bloch wave number and Λ is the period of the structure. This results in,

$$\cos(K\Lambda) = \frac{1}{2}(M_{B11} + M_{B22}). \tag{8}$$

The real solutions of this eigenvalue equation give the transmission bands of the layered structure, which can be easily determined by solving $|\frac{1}{2}(M_{B11} + M_{B22})| \leq 1$. The upper bound of those transmission bands can be expected to be excited by a uniform illumination of the structure, and show a good prediction of the propagation constants e.g. the effective refractive index of the material system. It is obvious, that due to the different coupling matrices for TE- and TM-polarization, the effective refractive index of the material system is polarization dependent.

3 Methods and Results

Before tackling the fabrication of the prisms, we wanted to study the guiding properties of the layered media. For this reason, we printed a rectangular array of periodic 300 µm-thick Polystyrene (PS) layers. Subsequently, we measured the frequency dependent refractive index of this composite material using a THz Time Domain Spectroscopy (THz TDS) system. The results, in Fig. 1, show a strong dispersion for frequencies between 200 and 500 GHz. Above 500 GHz scattering due to structural roughness becomes significant for the devices fabricated with our 3D printer. We therefore restrict ourselves to frequencies below 500 GHz for this analysis.

We printed three non-adjustable prisms first. These prisms had 200, 400 and 600 µm-thick air gaps between the PS layers. For technical reasons, we had to increase the layer thicknesses to 400 µm in order to obtain uniform layers. A periodic array of 400 µm-thick triangular layers, with an apex angle $\alpha = 53.13°$ and a $35 \times 35\,\mathrm{mm}^2$ base area make up the prisms as shown in Fig. 2. All samples were fabricated by an Ultimaker 3D printer with a slightly increased volumetric flow in order to print layers with uniform thickness. All printing jobs were done with commercial PS filaments and took from 10 to 15 hours.

For the characterization, the different prisms were placed on the axis of a goniometer in order to measure the deflection of the incident light with the aid of a THz TDS system as shown in Fig. 3 (see [16] for further details on the setup). Measurements of the intensity as a function of the frequency and the output angle are shown in Fig. 4(a) where the intensity is represented with a false-color scale. Note, that only relative values for the intensity are given since we were interested in the functionality of the device and not in its absolute efficiency. In Fig. 4(b), the intensity as a function of the angle is plotted for 700 GHz, 250 GHz and 150 GHz for all three prisms.

From these results one can see that a prism shaped device made out of a layered media indeed shows dispersion in the THz frequency range. This is particularly

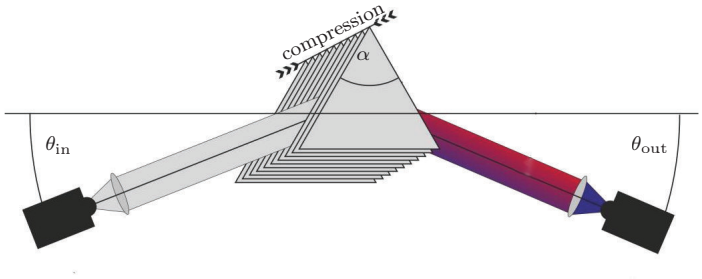

Fig. 3 Illustration of the experimental setup showing the samples placed over the axis of a goniometer. The transceivers of a standard THz TDS system with fiber coupled antennas were placed on the arms of the goniometer, with the transmitter under a fixed angular position of $\theta_{in} = 10°$.

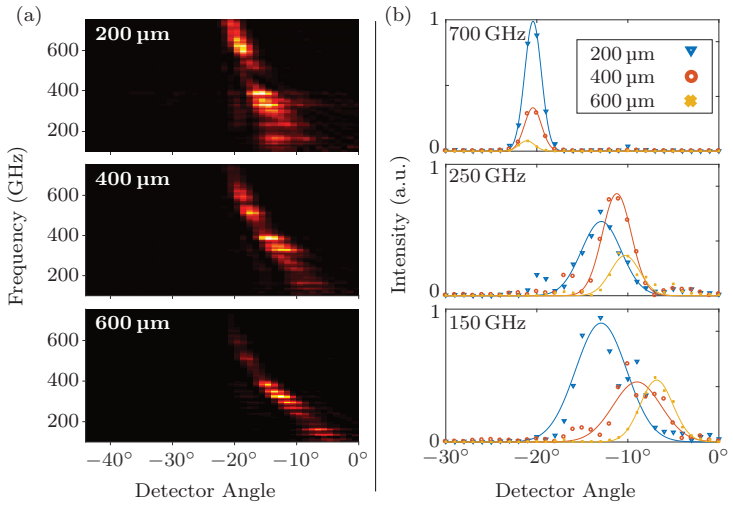

Fig. 4 Measurements of the intensity for three different prisms with 200, 400 and 600 µm-thick air gaps. (a) Intensity as a function of the frequency and output angle θ_{out}. (b) Angle-resolved beam profile for 700, 250 and 150 GHz. The fitted curves show the main deflection directions.

true for frequencies below 400 GHz where the intensity curves in Fig. 4(a) have a gradual slope. In consequence, close frequency values are measured at different angles. In the same way, a lower slope is obtained for air gaps greater than 200 µm. All these were further verified by the angle-resolved measurements of the beam profile in Fig. 4(b).

We now come to the tunable prism. It is constructed by printing a similar structure but with layers connected on the sides forming bow springs, as shown in Fig. 5. The measured refractive index is shown in Fig. 6. The dotted and the solid curves represent the TE and TM polarizations respectively, measured for different air gap values. Gray lines represent the simulations results as in Fig. 1.

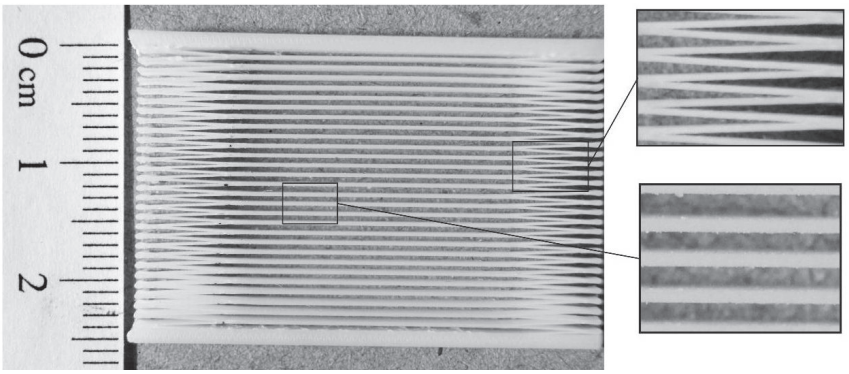

Fig. 5 Picture of a 3D printed tunable prism. Close-ups on the right show the ends of the layers articulated by joints that act as springs, and parallel slabs at the center in the same way as the fixed-size prisms.

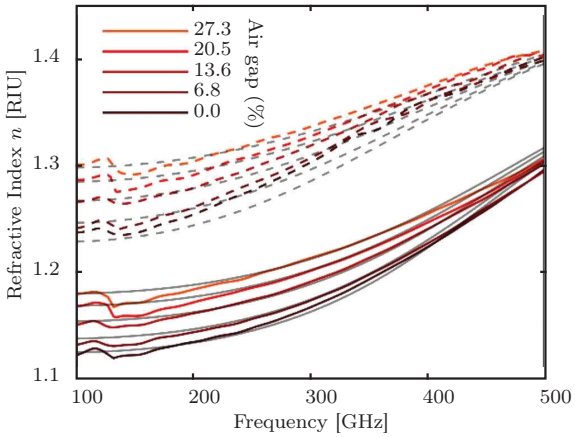

Fig. 6 Measurements for the refractive index for different air gap values. The dotted and solid curves represent TE and TM input polarizations respectively. Gray lines represent the numerical simulations as in Fig. 1.

In the same way, measurements of the intensity as a function of the frequency and the output angle θ_{out} were done for two different scenarios: the totally expanded prism and the totally compressed prism. These cases correspond to an air gap of 100 µm and 0 µm respectively, as shown in Fig. 7. In Fig. 7(a), a surface plot shows the different results for the two different cases. In Fig. 7(b), the angle-resolved beam profile is shown for three different frequencies: 700 GHz, 255 GHz and 155 GHz. Here one can see that the air gap values are irrelevant for 700 GHz. While for lower frequencies the air gaps have a strong dispersive effect. Also, for smaller air gaps, the peaks are shifted towards more negative angular values.

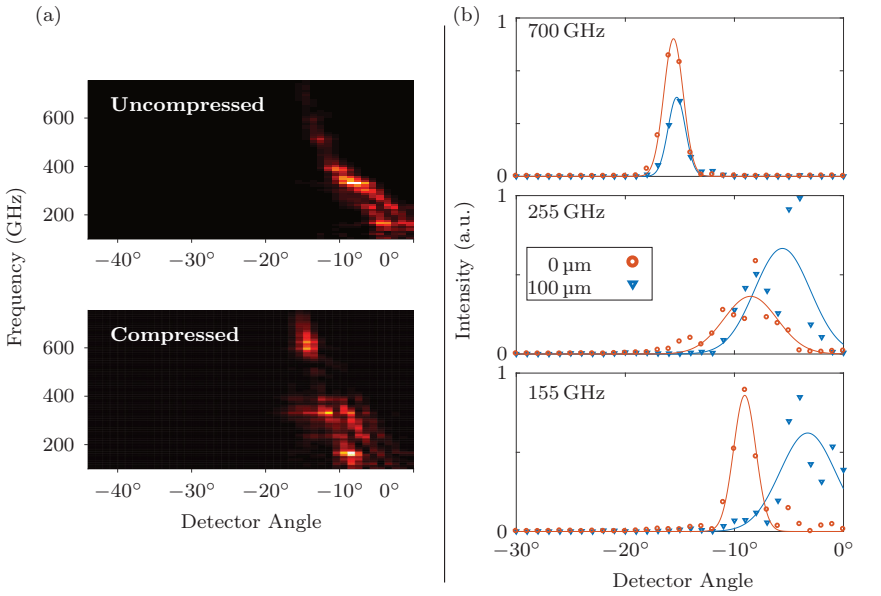

Fig. 7 Measurements of the intensity for the adjustable prism using a THz TDS as in Fig. 4. (a) Results for the intensity measured for an uncompressed and totally compressed prism as a function of the output frequency and output angle. (b) Angle-resolved beam profile measured for the same two cases as shown in the legend.

4 Conclusions

As expected, the dispersion caused by the anisotropy of the layered media will be more evident for higher frequencies (smaller wavelengths) relative to the thickness of the layers. As the frequency increases, the wavelength is small enough to be affected by the irregularities of the medium. Clearly, this effect will be frequency dependent, causing the steep slope for higher frequencies as seen on Fig. 1 and Fig. 6. This is further supported by the good resemblance observed between the numerical and experimental results for the effective refractive index.

In addition, the output intensity was measured as a function of the frequency and the output angle by using THz TDS system for frequencies between 100 and 700 GHz. As shown by Fig. 4 and Fig. 7, the results show clearly a frequency dependent structured material. A considerable frequency dependence is also evident from the surface plots in Fig. 4(a) and Fig. 7(a). The parabola-like spectra show a steeper behavior for angles close to 20°. Conversely, Fig. 4(b) and Fig. 7(b) show that for lower frequencies, the air gap has a stronger effect.

Summing up, we have constructed a tunable device that is able to spatially separate the different frequency components of a THz pulse. This prism was designed by using an analytical approach and, moreover, we have presented an experimental design of a mechanically tunable semi-optical prism. The experimental results show that these prisms are not only effective and robust, but also easy to fabricate, lightweight, durable, compact and inexpensive in comparison with previous studies.

Acknowledgements The authors will like to acknowledge Kirsti Krüger for the pictures of the 3D printed devices in Fig. 2 and Fig. 5. F. Beltran-Mejia acknowledges support from Finep/Funttel (01.14.0231.00) under the Radiocommunication Reference Center – CRR, project of the National Institute of Telecommunications – Inatel, Brazil.

References

1. S.F. Busch, M. Weidenbach, M. Fey, F. Schäfer, T. Probst, M. Koch, J. Infrared Milli. Terahz. Waves **35**(12), 993 (2014)
2. B. Scherger, M. Scheller, C. Jansen, M. Koch, K. Wiesauer, Appl. Opt. **50**(15), 2256 (2011)
3. B. Scherger, C. Jördens, M. Koch, Opt. Express **19**(5), 4528 (2011)
4. K. Szkudlarek, M. Sypek, G. Cywiński, J. Suszek, P. Zagrajek, A. Feduniewicz-Żmuda, I. Yahniuk, S. Yatsunenko, A. Nowakowska-Siwińska, D. Coquillat, D.B. But, M. Rachoń, K. Węgrzyńska, C. Skierbiszewski, W. Knap, Opt. Express **24**(18), 20119 (2016)
5. K. Liebert, M. Rachon, A. Siemion, J. Suszek, D. But, W. Knap, M. Sypek, J. Infrared Milli. Terahz. Waves **38**(8), 1019 (2017)
6. R. Mendis, D. Grischkowsky, J. Appl. Phys. **88**(7), 4449 (2000)
7. A. Hassani, A. Dupuis, M. Skorobogatiy, Opt. Express **16**(9), 6340 (2008)
8. K. Nielsen, H.K. Rasmussen, A.J.L. Adam, P.C.M. Planken, O. Bang, P.U. Jepsen, Opt. Express **17**(10), 8592 (2009)
9. S. Atakaramians, S.A. V, T.M. Monro, D. Abbott, Adv. Opt. Photon. **5**(2), 169 (2013)
10. D.W. Vogt, R. Leonhardt, J. Infrared. Milli. Terahz. Waves pp. 1–10 (2016)
11. B. Scherger, N. Born, C. Jansen, S. Schumann, M. Koch, K. Wiesauer, IEEE Trans. THz Sci. Technol. **2**(5), 556 (2012)
12. S.F. Busch, M. Weidenbach, J.C. Balzer, M. Koch, J. Infrared. Milli. Terahz. Waves **37**(4), 303 (2016)
13. D. Jahn, M. Weidenbach, J. Lehr, L. Becker, F. Beltran-Mejia, S.F. Busch, J.C. Balzer, M. Koch, J. Infrared Milli. Terahz. Waves **38**(6), 708 (2017)
14. C. Jördens, K.L. Chee, I.A.I. Al-Naib, I. Pupeza, S. Peik, G. Wenke, M. Koch, J. Infrared Milli. Terahz. Waves **31**(2), 214 (2009)
15. M. Weidenbach, D. Jahn, A. Rehn, S.F. Busch, F. Beltran-Mejia, J.C. Balzer, M. Koch, Opt. Express **24**(25), 28968 (2016)
16. C. Goy, M. Scheller, B. Scherger, V.P. Wallace, M. Koch, Opt. Express **21**(16), 19292 (2013)
17. T. Prasad, V.L. Colvin, Z. Jian, D.M. Mittleman, Opt. Lett. **32**(6), 683 (2007)
18. A.I. Hernandez-Serrano, E. Castro-Camus, J. Infrared. Milli. Terahz. Waves **38**(5), 567 (2017)
19. N.J. Karl, R.W. McKinney, Y. Monnai, R. Mendis, D.M. Mittleman, Nat. Photonics **9**(11), 717 (2015)
20. R.C. Enger, S.K. Case, Appl. Opt. **22**(20), 3220 (1983)
21. B. Päivänranta, N. Passilly, J. Pietarinen, P. Laakkonen, M. Kuittinen, J. Tervo, Opt. Express **16**(21), 16334 (2008)
22. S.C. Saha, Y. Ma, J.P. Grant, A. Khalid, D.R.S. Cumming, in *2010 IEEE Photonics Society Winter Topicals Meeting Series (WTM)* (2010), pp. 38–39
23. B. Scherger, M. Scheller, N. Vieweg, S.T. Cundiff, M. Koch, Opt. Express **19**(25), 24884 (2011)
24. S.G. Johnson, J.D. Joannopoulos, Opt. Express **8**(3), 173 (2001)
25. P. Yeh, A. Yariv, C.S. Hong, J. Opt. Soc. Am. **67**(4), 423 (1977)